Available online at www.sciencedirect.com
SCIENCE DIRECT®
Journal of Sound and Vibration 287 (2005) 77–100
JOURNAL OF SOUND AND VIBRATION
www.elsevier.com/locate/jsvi

Free vibration of cellular structures using continuum modes

Sourish Banerjee, Atul Bhaskar*

School of Engineering Sciences, University of Southampton, Southampton SO17 1BJ, UK

Received 11 December 2003; received in revised form 12 August 2004; accepted 26 October 2004
Available online 22 January 2005

Abstract

This paper is concerned with free vibration of elastic structures made up of cellular material. A network of cells in a plane is considered. Cell walls are modelled as beams. The problem of calculating the first few natural frequencies and the corresponding mode shapes is addressed. An approximate method based on the assumption that cellular solids behave as a continuum for low-frequency dynamics is presented. A direct application of the assumed modes method incorporating continuum modes as basis leads to difficulties. The source of this difficulty is identified. A method that uses inverse power iterations is proposed to pre-condition the assumed modes appropriately. The proposed method of using continuum modes as basis for model order reduction leads to substantial computational saving while maintaining good accuracy. Two examples are given to illustrate the proposed procedure of using the continuum modes in conjunction with pre-conditioning.

1. Introduction

Cellular materials are increasingly being used for structural applications. Wood, cork and bone are common examples of solids that contain substantial porosity. At the mesoscopic scales of length the material exhibits a complex network of elastic elements. Many artificial materials share the same generic features at this level: polymeric, ceramic and metallic foams and honeycombs are perhaps industrially most important. Often porous metal and honeycombs are used as the core material in sandwich constructions. These constructions exhibit high stiffness to weight ratio—a

*Corresponding author.
E-mail address: a.bhaskar@soton.ac.uk (A. Bhaskar).

0022-460X/$ - see front matter © 2004 Elsevier Ltd. All rights reserved.
doi:10.1016/j.jsv.2004.10.051

very useful property for aeronautical applications. Packaging, thermal insulation, acoustic damping etc. are other common applications.

When such a material is used for constructing structures that have dimensions much larger than typical cell dimensions, the material can be conceived to be homogeneous with some effective elastic properties. These effective properties primarily depend on the cell-size, its distribution, the cell wall material and the topology of the cells. The existing literature on the mechanics of cellular materials is mainly devoted to the understanding of the elastic behaviour of the cellular solids under static loads. Analytical and experimental methods have been used. The main aim of these studies was to calculate the effective mechanical properties and their dependence on the effective density and the topology of the microstructure. Gibson et al. [1] were the first to give a comprehensive account of the in-plane elastic and the plastic behaviour of the cellular solids made of hexagonal cells. They used the *unit cell approach* and determined the elastic constants for lattices with hexagons when bending deformations of the cell walls are dominant.

Warren and Kraynik [2] developed expressions for elastic constants of regular hexagonal honeycombs using kinematic arguments. They included both the axial and the bending deformations of the cell walls. Gulati [3] evaluated expressions for elastic constants of honeycombs made of triangular cells using an energy approach. Scarpa et al. [4] studied the effect of uni-axial in-plane loading on honeycombs made of inverted hexagons using the finite element method and experiments.

Menges and Knipschild [5] derived expressions for the modulus of elasticity considering bending and axial deformations of the cell edges. Works of Menges and Knipschild [5] and Ko [6] identified bending of the cell walls as the dominant mechanism of deformation in foams.

A wide range of mechanical properties e.g. elastic, plastic, buckling, thermal conductivity etc. have been discussed in the work of Gibson and Ashby [7]. Discussions about the mechanical behaviour of open and closed cell foams can be found in Gibson's review [8] on metallic foams. Christensen [9] surveyed the relationship between the mechanical properties, effective density and the various cell-shapes for two- and three-dimensional cellular materials. Grenestedt's work [10] analysed the various models used to study the mechanics of cellular solids without any imperfections.

Silva et al. [11] have studied the effect of microstructural variability on the elastic behaviour of two-dimensional cellular solids using the finite element method. Their results show that, for the same relative density, the average elastic properties of the irregular and the regular hexagonal honeycombs are almost the same. They have also studied the effect of directionally oriented irregularity on the elastic anisotropy for irregular honeycombs. Zhu et al. [12] studied the dependence of elastic properties on the degree of irregularity of the microstructure. They showed that the effective elastic and shear modulus can vary by up to 20% from the values of modulii for regular hexagons of the same relative density.

In another study, Silva et al. [13] studied the effect of the local defects (e.g. removal of cell walls) in the random microstructure on the bulk compressive failure behaviour. The effects of imperfections, such as the wavy nature of the cell walls, thickness variation of the cell walls and missing cells on the elastic and yielding behaviour have been studied by Simone and Gibson [14], Grenestedt [15] and Chen et al. [16].

For irregular honeycombs or foams, simulation of the real microstructure becomes important. Hollister and Kikuchi [17] used information from digital images in their finite element simulations

to study the effect of microstructural morphology of bones. Garboczi and Day [18] developed an algorithm to calculate the effective elastic properties of random multi-phase materials. They treated each pixel of the digital image as a linear finite element.

Homogenisation theory has also been applied in the study of the cellular solids to determine the effective properties. Torquato et al. [19] compared the bounds on effective properties with the results obtained from the finite element calculations.

Although there are several studies on the statics of cellular materials, the dynamics of this class of solids does not appear to have received much attention. Wang and Stronge [20] studied elastic regular hexagonal honeycombs under periodically fluctuating forces using the micropolar theory. Baker et al. [21] studied the effect of impact and energy absorption of metal honeycombs. To the best of our knowledge, no work has so far has been reported on the vibration of cellular materials. Since structures made of these materials are frequently used under dynamic environment, there is a need to understand the dynamic behaviour. The present study is motivated by this need.

When a structure is made up of small cells, a field description in the spirit of the theory of elasticity is impractical due to the complexity of the internal geometry. Therefore, in this paper, the overall structure is modelled as a finite element assembly. The cell walls are modelled as elastic beams. Since a typical cell is much smaller than the overall dimensions of the structure, several beam elements are required for detailed description. Supposing that the description is available either by analytical method or by digital image based techniques, the number of degrees-of-freedom of the overall structure will then be very large. In this circumstance, the eigenvalue problem resulting from the free vibration analysis is large—hence computationally expensive.

The main contribution of this paper is in reducing the computational expense for calculations related to free vibration of a cellular structure. This is achieved in the spirit of model order reduction with the so-called *continuum modes* used as the basis. The method preserves all the structural details via complete mass and stiffness matrices but the resulting full-scale eigensolution is done away with. This method could be used when one is interested in the low-frequency dynamics. Low- and high-frequency regions can be best characterised using the wavelength of the standing waves for a given normal mode. When this wavelength is much greater than typical cell size, the corresponding natural frequency will be referred to as 'low frequency'—a band in which the proposed approximation of this paper is valid. The actual values of the frequency is unimportant since the validity of the approximation does not depend on this. In this way we will use the word low frequency and long wavelength synonymously. For high-frequency dynamics, a piece of cellular solid ceases to behave as a continuum and the proposed method is not suitable in that case. It is found that a direct model order reduction possesses difficulties. It is then shown in this paper that this difficulty can be attributed to the presence of small components in the assumed modes that are associated with exceptionally high frequencies. A method to remove these high-frequency components from the assumed modes is proposed.

It is not our aim to model a given piece of cellular material in detail. On the contrary, we assume that such a model is available to us—we focus our attention to the problem of reducing computational expense while maintaining accuracy. For simplicity, the illustrative examples given in this paper are two-dimensional—a compromise as far as exactness of modelling is concerned.

The paper is organised as follows. An approximation for low-frequency dynamics of cellular structures is presented in the next section. It is realised there that a direct application of the assumed modes method that uses continuum modes is prone to large errors. A method based on

inverse power iterations is presented in Section 3. Two examples that demonstrate the proposed method in this paper are given in Section 4. Finally, conclusions are drawn in Section 5.

2. An approximation for cellular structures based on continuum modes

Structures made up of elastic cells are analysed in this paper. The finite element method has been used to obtain a discrete model. Each cell wall is modelled as a two-node elastic beam. It is possible to use more elements to represent a cell wall to improve accuracy, however, for low-frequency dynamics it is not critical. It is assumed that all the cell walls have uniform thickness. Damping in the cell walls is neglected. Small amplitude vibration is considered—this justifies a linear analysis. The effect of shear in the cell walls is ignored in the analysis. This is a valid assumption for studying the first few modes of the overall structure because the deflections at the cell wall level do not take a very rapidly fluctuating shape.

Euler–Bernoulli beam theory is employed for analysis. Stretching as well as bending deformations in the beams are included in the model. The global stiffness matrix $\mathbf{K}$ and the global inertia matrix $\mathbf{M}$ are assembled in the usual way [22]. Note that $\mathbf{K}$ and $\mathbf{M}$ incorporate all the structural details. Let $\boldsymbol{\eta}(t)$ represent the vector of generalised coordinates of the whole structure. The kinetic energy $T(t)$ and the potential energy $V(t)$ are expressed as

$$T(t) = \tfrac{1}{2}\dot{\boldsymbol{\eta}}^{\mathrm{T}}\mathbf{M}\dot{\boldsymbol{\eta}}, \quad V(t) = \tfrac{1}{2}\boldsymbol{\eta}^{\mathrm{T}}\mathbf{K}\boldsymbol{\eta}. \tag{1}$$

For a conservative system, Lagrangian L is in the form $L = T - V$. Applying Hamilton's principle, first variational of the integral of the Lagrangian between time interval t_1 and t_2 is zero, i.e. $\delta \int_{t_1}^{t_2} L\,\mathrm{d}t = 0$, the set of equations of motion are obtained as

$$\mathbf{M}\ddot{\boldsymbol{\eta}} + \mathbf{K}\boldsymbol{\eta} = \mathbf{0}. \tag{2}$$

Looking for synchronous free vibration, the above equation leads to the following algebraic eigenvalue problem

$$\mathbf{K}\mathbf{u}_r = \lambda_r \mathbf{M}\mathbf{u}_r, \tag{3}$$

where λ_r is the rth eigenvalue, and $\mathbf{u}_r$ is the corresponding eigenvector. Square root of the eigenvalue λ_r is a natural frequency ω_r of the overall structure. Usually the eigenvalue problem (3) is of very large size when the structure is modelled realistically.

Porous solids are not homogeneous at the scales of length comparable to the size of a typical cell. At this level, a piece of cellular material is a complex network of elastic elements. Therefore, for dynamics that involve short waves, a cellular structure exhibits all the local details at the cell level and the behaviour has a strong local influence. On the other hand, for dynamics at low frequency, usually associated with long waves, the behaviour at the bulk level resembles continuum behaviour with the effective properties of the continuum that depend on the statistical distribution of elastic members.

A structure made up of cellular material possesses geometrical features at two length scales. First, the scale of length of the overall structure, say l_s, is typically represented by the characteristic length in a hypothetical solid when the porosity is completely filled. Second, the scale of length of the porosity or cells, say l_c, is assumed to be small, i.e. $l_c \ll l_s$. We also assume

that we are interested in the dynamics at a length scale much greater than l_c which means that the wavelengths involved are much longer than l_c. In these circumstances, we can guess the mode shape of the overall structure by filling the porosity and treating the structure as a homogeneous medium at the length scale l_s. Since the mode shapes do not strongly depend on the material properties, it does not matter what properties (in terms of the elastic modulus and density) are chosen while calculating the guessed mode shape. Once the mode shapes of the hypothetical medium, to be called *continuum modes* in future, are calculated, the mode shapes of the cellular structure are interpreted by mapping the displacement and rotation fields of this hypothetical porosity filled structure onto the nodes where cell walls join each other.

The last step of interpreting mode shapes of a cellular structure based on those of a continuum structure requires simple kinematic calculations. In engineering practice, the overall structures are often made of simpler elements such as plates, beams or shells. In that case, the calculation of the continuum modes will be greatly simplified. For example, if we have a planar cellular structure made up of beams at the length scales l_s, then we need to consider only the skeleton of beams to calculate the modes of a structure made of a hypothetical homogeneous medium. The displacement field at other points can be calculated by using the kinematic relations intrinsic to the beam theory, i.e. plane sections remain plane and normal to the skeleton axis.

In our numerical implementations, we have restricted ourselves to planar structures with cell walls modelled as beams. The skeleton at length scales l_s is also modelled using beam elements. These beams have axial degrees of freedom in addition to the transverse displacement and rotation at each of the two nodes of an element. In a local coordinate system, the transverse displacement $\phi(x)$ is approximated using the four Hermite cubics. The displacement and rotation fields within an element are then given by

$$v_x^b(x,y) = -y\,\frac{\mathrm{d}\phi}{\mathrm{d}x}, \quad v_y(x) = \phi(x), \quad \theta(x) = \frac{\mathrm{d}\phi}{\mathrm{d}x}, \tag{4}$$

where $v_x^b(x,y)$ is the displacement in the axial direction of the element due to bending effects only, $v_y(x)$ is the transverse displacement of the neutral axis which is the transverse displacement of all the points normal to the neutral axis, and $\theta(x)$ is the rotation of the cross-section. The total displacement field is obtained by superposing the displacement in the axial direction due to tension–compression effects, i.e.

$$v_x(x,y) = v_x^b(x,y) + v_x^{\text{tension}}(x). \tag{5}$$

Note that v_x^{tension} is assumed to be a function of x alone which asserts that this displacement component is distributed uniformly through the cross-section: an assumption consistent with one-dimensional rod theories. This component is calculated by interpolating the axial displacement field from the nodal axial displacements.

There will be a transverse displacement field $v_y^{\text{tension}}(x)$ due to Poisson's ratio effect. However, we have ignored this part of the displacement field in obtaining the assumed modes for two reasons: firstly, the contribution to the overall displacement from tension–compression is usually small since rods are stiff in tension–compression than in bending. Secondly, there is no way to know the effective Poisson's ratio of the cellular material at the start of the calculations.

Having obtained the nodal displacements of the elements used to model the skeleton, Eqs. (4) and (5) enable us to calculate the displacement and rotation fields at any point within the

structure, as though the structure were made of homogeneous material. We use these kinematic relations now to map the displacement field $v_x(x), v_y(x), \theta(x)$ onto the displacements at the joints of the cell walls in the actual cellular structure, i.e.

$$\{v_x, v_y, \theta(x)\} \mapsto \mathbf{q}_{\text{joints}}. \tag{6}$$

The generalised displacement vector at the joints contains displacements in the plane and rotation. We will denote these components for the complete structure as obtained for the ith mode of the structure by $\mathbf{q}_i$. We assume that the necessary coordinate transformations have been employed so that $\mathbf{q}_i$ is expressed in a global coordinate system.

Starting with p number of assumed modes $\mathbf{q}_i$, $i = 1, 2, \ldots, p$ we are now in a position to build a reduced order model of size $p \times p$. To achieve this, we express the N-dimensional vector of generalised co-ordinates $\mathbf{q}$ in terms of the assumed modes $\mathbf{q}_i$ as

$$\mathbf{q} = \sum_{i=1}^{p} c_i \mathbf{q}_i. \tag{7}$$

This expansion can be seen as the following transformation:

$$\mathbf{q} = \mathbf{T}\mathbf{c}, \tag{8}$$

where the $N \times p$ transformation matrix $\mathbf{T}$ is the matrix whose columns are $\mathbf{q}_i$, i.e.

$$\mathbf{T} = [\mathbf{q}_1 | \mathbf{q}_2 | \ldots | \mathbf{q}_p]. \tag{9}$$

The vector $\mathbf{c}$ is of length p and contains $c_1, c_2, \ldots, c_p$ in a column.

Rayleigh's quotient in terms of $\mathbf{q}$ as the trial vector is now given by

$$R = \frac{\mathbf{q}^{\mathrm{T}}\mathbf{K}\mathbf{q}}{\mathbf{q}^{\mathrm{T}}\mathbf{M}\mathbf{q}}, \tag{10}$$

where $\mathbf{K}$ and $\mathbf{M}$ are the $N \times N$ stiffness and mass matrices, respectively, of whole structure. Note that these matrices contain all the detailed information about the geometry, properties and topology of the network of beams at the cell level.

Substituting the transformation (8) into (10) we have

$$R = \frac{\mathbf{c}^{\mathrm{T}}\mathbf{T}^{\mathrm{T}}\mathbf{K}\mathbf{T}\mathbf{c}}{\mathbf{c}^{\mathrm{T}}\mathbf{T}^{\mathrm{T}}\mathbf{M}\mathbf{T}\mathbf{c}}. \tag{11}$$

Thus, Rayleigh's quotient is a ratio with c_i, $i = 1, 2, \ldots, p$ as the unknowns. Applying Rayleigh's variational principle, the first variation of this quotient must be zero, i.e. $\delta R(c_1, c_2, \ldots, c_p) = 0$. This amounts to setting the first derivative of R with respect to each of the unknowns to zero, i.e.

$$\frac{\partial R}{\partial c_i} = 0, \quad i = 1, 2, \ldots, p. \tag{12}$$

Since both the numerator and the denominator of R are quadratic forms, application of condition (12) leads to the following eigenvalue problem

$$\overline{\mathbf{K}}\mathbf{c} = \mu\overline{\mathbf{M}}\mathbf{c}, \tag{13}$$

where $\overline{\mathbf{K}} = \mathbf{T}^{\mathrm{T}}\mathbf{K}\mathbf{T}$ and $\overline{\mathbf{M}} = \mathbf{T}^{\mathrm{T}}\mathbf{M}\mathbf{T}$. This eigenproblem is of size p. Assuming that $p \ll N$, we conclude that the reduced order model will save substantial computation since we do not need to solve the full-scale eigenproblem (3) of size N.

Solution of the eigenvalue problem (13) gives p number of eigenvalues μ_r, $r = 1, 2, \ldots, p$ and the corresponding eigenvectors $\mathbf{c}_1, \mathbf{c}_2, \ldots, \mathbf{c}_p$. The eigenvalues μ_r are approximations for the exact eigenvalues λ_r and the eigenvectors $\mathbf{c}_r$ contain information about the corresponding mode shapes $\mathbf{q}_r$. Mode shapes of the overall structure are calculated for each $\mathbf{c}_r$ by substituting the components of these vectors into the summation (7). As can be seen that the reduced order eigenproblem (13) affords only p number of modal parameters instead of the complete set of N, but this is the price that one has to pay for computational economy. Often this will be satisfactory because in many practical situations, the excitation occurs over a band of frequency and hence one needs to consider modes only within (and slightly outside) this band.

When only one assumed mode is used in the summation (7), it amounts to substitution of the assumed mode for the trial vector $\mathbf{q}$ in Eq. (10). The accuracy of this approximation depends on the closeness of the assumed mode to the actual mode. It is a well-known property of Rayleigh's quotient that if the trial vector $\mathbf{q}$ differs from an eigenvector (say, $\mathbf{u}_r$) by an amount of the order of a small quantity, say ε, then Rayleigh's quotient for this trial vector differs from the corresponding eigenvalue by an amount of the order of ε^2. Thus eigenvalue estimates are more accurate than the trial vectors used in Rayleigh's quotient approximation. While using the continuum modes we find that the assumed modes are indeed very close to the actual modes (the difference, say, being of the order of ε), still the frequencies are poorly predicted by a direct application of Rayleigh's approximation. We will look into the approximation more closely in the next section. We will also propose a method to overcome the difficulty identified.

3. Rayleigh's variational method and pre-conditioning of the trial modes

We turn to the single mode approximation first. It will be assumed that the trial mode is close to the actual mode shape. Expanding the trial vector $\mathbf{q}$ in terms of the eigenvectors of the original eigenproblem (3), we have

$$\mathbf{q} = b_1\mathbf{u}_1 + \cdots + b_i\mathbf{u}_i + \cdots + b_N\mathbf{u}_N, \tag{14}$$

where N is the size of the original eigenproblem and $b_1, b_2, \ldots, b_N$ are constants. For the ease of presentation of analysis, we assume that the trial mode resembles the first mode shape $\mathbf{u}_1$ and is corrupted by contribution from a single mode $\mathbf{u}_m$ so that

$$\mathbf{q} = a_1\mathbf{u}_1 + a_m\mathbf{u}_m. \tag{15}$$

Further, assuming that the contribution from the mth mode is small compared to that from the first mode (the mode whose frequency is being estimated by the approximation), we set $a_1 = 1$ and $a_m = \varepsilon$ with $\varepsilon \ll 1$. Substituting for $\mathbf{q}$ in the expression of R in Eq. (10) we have

$$R = \frac{(\mathbf{u}_1^{\mathrm{T}} + \varepsilon\mathbf{u}_m^{\mathrm{T}})\mathbf{K}(\mathbf{u}_1 + \varepsilon\mathbf{u}_m)}{(\mathbf{u}_1 + \varepsilon\mathbf{u}_m^{\mathrm{T}})\mathbf{M}(\mathbf{u}_1 + \varepsilon\mathbf{u}_m)}. \tag{16}$$

We assume that the eigenvectors $\mathbf{u}_r$ are mass-normalised, so that the orthogonality relationship gives $\mathbf{u}_i^{\mathrm{T}}\mathbf{M}\mathbf{u}_j = \delta_{ij}$ and $\mathbf{u}_i^{\mathrm{T}}\mathbf{K}\mathbf{u}_j = \lambda_i\delta_{ij}$, $i,j = 1,m$, where δ_{ij} is the Kronecker-delta. Substituting the above in Eq. (16), after some algebra we obtain

$$R = \frac{\lambda_1 + \varepsilon^2\lambda_m}{1+\varepsilon^2}. \tag{17}$$

If $\lambda_1 = o(\lambda_m)$, then $R = \lambda_1 + o(\varepsilon^2)$. However, if $\lambda_m \gg \lambda_1$, then the difference $R - \lambda_1$ can become very large affecting the approximation adversely. Suppose $\lambda_m/\lambda_1 = M \gg 1$, then $R \approx \lambda_1(1+\varepsilon^2 M)$, and therefore, $R - \lambda_1 \approx \lambda_1\varepsilon^2 M \neq o(\varepsilon^2)$.

The above analysis is restricted to a single mode approximation. The case of an approximation involving several continuum modes $\mathbf{q}_1, \mathbf{q}_2, \ldots$ can be treated similarly. Again for simplicity, we assume that there are only two modes to be used in the approximation (i.e. $p = 2$) and that each mode is corrupted by a small amount whose contribution comes from the mth mode, $m \gg 2$. Expressing this mathematically, we have

$$\mathbf{q}_1 = \mathbf{u}_1 + \varepsilon\mathbf{u}_m, \quad \mathbf{q}_2 = \mathbf{u}_2 + \varepsilon\mathbf{u}_m. \tag{18}$$

Assuming $\mathbf{u}_1, \mathbf{u}_2, \mathbf{u}_m$ to be mass normalised, the transformation matrix $\mathbf{T}$ as in Eq. (9) takes the form

$$\mathbf{T} = [(\mathbf{u}_1 + \varepsilon\mathbf{u}_m)|(\mathbf{u}_2 + \varepsilon\mathbf{u}_m)]. \tag{19}$$

Substituting this into the expressions following Eq. (13), the 2×2 matrices are obtained as

$$\overline{\mathbf{K}} = \begin{bmatrix} (\lambda_1 + \varepsilon^2\lambda_m) & \varepsilon^2\lambda_m \\ \varepsilon^2\lambda_m & (\lambda_2 + \varepsilon^2\lambda_m) \end{bmatrix}, \quad \overline{\mathbf{M}} = \begin{bmatrix} (1+\varepsilon^2) & \varepsilon^2 \\ \varepsilon^2 & (1+\varepsilon^2) \end{bmatrix}. \tag{20}$$

The eigenvalues μ can be obtained in closed form from the following quadratic equation:

$$A\mu^2 + B\mu + C = 0, \tag{21}$$

where $A = (1+2\varepsilon^2)$, $B = -[(1+\varepsilon^2)(\lambda_1+\lambda_2) + 2\lambda_m\varepsilon^2]$ and $C = \lambda_1\lambda_2 + \varepsilon^2\lambda_m(\lambda_1+\lambda_2)$. Solving this quadratic we have

$$\mu_{1,2} = \frac{[(1+\varepsilon^2)(\lambda_1+\lambda_2) + 2\varepsilon^2\lambda_m] \pm \sqrt{(1+\varepsilon^2)^2(\lambda_1-\lambda_2)^2 + 4\varepsilon^4[\lambda_m^2 - \lambda_m(\lambda_1+\lambda_2) + \lambda_1\lambda_2]}}{2(1+\varepsilon^2)}. \tag{22}$$

When ε is small but λ_m is large, i.e. when $\varepsilon \to 0$ and $\lambda_m \gg \lambda_2 > \lambda_1$ then

$$\mu_{1,2} = \left(\frac{\lambda_1+\lambda_2}{2}\right), \quad \left(\frac{\lambda_1+\lambda_2}{2} + \varepsilon^2\lambda_m\right). \tag{23}$$

This confirms that the two approximate eigenvalues μ_1 and μ_2 do not resemble the actual eigenvalues λ_1 and λ_2 in the circumstances. When we implemented the method outlined in Section 2, we observed that the errors in the estimation of approximate eigenvalues μ were often very large. To understand this further we present the following sensitivity analysis to study the rate of change of the approximate eigenvalues with respect to change in the parameter ε. To do this we view the eigenproblem (13) as one that depends on the parameter ε. In that case, the eigenvalues have the functional relationship $\mu_i = \mu_i(\varepsilon)$. Fortunately, we can estimate the derivative of an eigenvalue exactly when an eigenproblem depends on a parameter [23]. The expression for the

eigenderivative is given in the present context by

$$\frac{\partial \mu_i}{\partial \varepsilon} = \frac{\mathbf{c}_i^{\mathrm{T}}[\partial \overline{\mathbf{K}}/\partial \varepsilon - \mu_i \partial \overline{\mathbf{M}}/\partial \varepsilon]\mathbf{c}_i}{\mathbf{c}_i^{\mathrm{T}} \overline{\mathbf{M}} \mathbf{c}_i}. \tag{24}$$

Since we know the functional dependences of $\overline{\mathbf{K}}(\varepsilon)$ and $\overline{\mathbf{M}}(\varepsilon)$ explicitly via Eq. (20), differentiation leads to

$$\frac{\partial \overline{\mathbf{K}}}{\partial \varepsilon} = 2\varepsilon\lambda_m \mathbf{1}, \quad \frac{\partial \overline{\mathbf{M}}}{\partial \varepsilon} = 2\varepsilon \mathbf{1} \tag{25}$$

where the 2×2 matrix $\mathbf{1}$ contains 1's everywhere. We now divide the above sensitivity relationship by (μ_i/ε) and define the non-dimensional ratio σ_i as the *relative sensitivity* for the ith mode to obtain

$$\sigma_i = \frac{(\partial \mu_i/\partial \varepsilon)}{(\mu_i/\varepsilon)} = \frac{2\varepsilon^2 \left(\dfrac{\lambda_m}{\mu_i} - 1\right) G}{(1+\varepsilon^2)}, \tag{26}$$

where

$$G = \frac{\mathbf{c}_i^{\mathrm{T}} \mathbf{1} \mathbf{c}_i}{\mathbf{c}_i^{\mathrm{T}} \mathbf{c}_i}.$$

Note that the number G is bounded in the range $0 < G < 2$ since G is a Rayleigh's quotient associated with the matrix $\mathbf{1}$ and since the eigenvalues of $\mathbf{1}$ are 0 and 2. As $\varepsilon \to 0$, both $\overline{\mathbf{M}}$ and $\overline{\mathbf{K}}$ become diagonal so that $\mathbf{c}_i$ is either $[0\ 1]^{\mathrm{T}}$ or $[1\ 0]^{\mathrm{T}}$. For these vectors, $G = 1$. Hence for $\varepsilon \ll 1$

$$\sigma_i \approx \frac{2\varepsilon^2((\lambda_m/\mu_i) - 1)}{(1+\varepsilon^2)}. \tag{27}$$

As in the previous cases of Eqs. (17) and (23), the smallness of ε^2 alone does not guarantee accuracy of the approximation: we require smallness of the term $\varepsilon^2\lambda_m$. Since the approximation method we have proposed uses the physical reasoning that the overall mode shapes must resemble those of a continuum, it is very difficult to control the contributions (however small) from higher modes. The case of cellular structures is a particularly difficult one because it requires building a very large model meaning that the eigenvalues of the complete structure span a large range, i.e. $\lambda_1 \ll \lambda_N$. This increases the chances of contributions coming from the high frequency end of the spectrum.

Having identified the difficulty, we now propose a way to help the situation by filtering the components corresponding to high frequencies from the assumed modes $\mathbf{q}_i$ before they are used either in Rayleigh's quotient (as in one mode approximation) or before they are used in the variational formulation of Eqs. (7)–(13). We propose to remove the high-frequency eigenmodes from the trial vectors by the use of inverse power iterations. When the power method of determining the dominant eigenvalue of a matrix is used, the method works by progressively enriching the iterated vector in favour of the large eigenvalue side of the spectrum. The contribution from the small eigenvalue side gradually becomes smaller as the iterations proceed. Since our aim is to determine the lowest few natural frequencies and the corresponding modes, we need to iterate with the inverse matrix. Fortunately, we do not need to compute the inverse

explicitly. All we need to do now is to cast the original eigenproblem (3) in the following form:

$$\frac{1}{\lambda}\,\mathbf{Kq} = \mathbf{Mq}. \tag{28}$$

The iterations at the rth step become

$$\mathbf{Kq}_i^{(r)} = \mathbf{Mq}_i^{(r-1)}, \tag{29}$$

where the superscript refers to the iteration number. The above set of algebraic equations needs to be solved for $\mathbf{q}_i^{(r)}$. The first vector $\mathbf{q}_i^{(0)}$ is the continuum mode presented in Section 2. In our numerical implementations, we found just one iteration to be sufficient. In spite of extra calculations involved in solving Eq. (29) and those involved in the mapping of Eq. (6), an overall saving in the total number of floating point operations was observed in our implementations.

4. Numerical examples and discussions

We now present two numerical implementations of the scheme of using continuum modes for the calculation of natural frequencies and normal modes for the first few modes. In the first instance we undertake a cantilever beam (see Fig. 1) made of cellular material. Then we present calculations for two cellular beams joined at right angle: we will refer to this structure as the L-beam (see Fig. 7).

4.1. Example 1: cantilever beam

Consider a cantilever beam clamped at the left end made up of cellular material (see Fig. 1). The network of beams representing cell walls was generated from a Voronoi diagram. The edges of each Voronoi cell represent cell walls.

Since the generation of these cells required randomly placed nucleation points for the Voronoi cells, there is a distribution of length of the cell walls. As a result, there is a small fraction of the total number of cell walls that is represented by short beams. This is undesirable from the point of view of mechanical modelling since the Euler–Bernoulli beam theory breaks down for very short beams. Since it is hard to control the length of the cell walls or the relative distance of the nucleation points with respect to close neighbours, we took an alternative approach of eliminating exceptionally short cell walls by moving the nodes so that the two ends of a short beam (shorter than a decided threshold) coalesce to a point. The connectivities with other neighbours for each of the two merging nodes is left unchanged. The threshold of discarding short beams was kept as the thickness t to length l ratio equal to 1:3. This ratio may appear as one representing very short beam, in practice there are very few beams of this t/l ratio. A large majority of cell walls (about

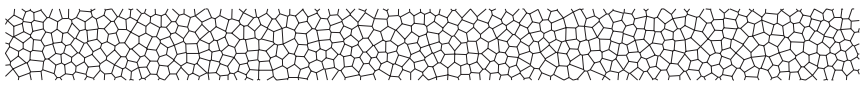

Fig. 1. A cellular beam. The microstructure is composed of irregular cells. Vibration in the plane of the paper is considered.

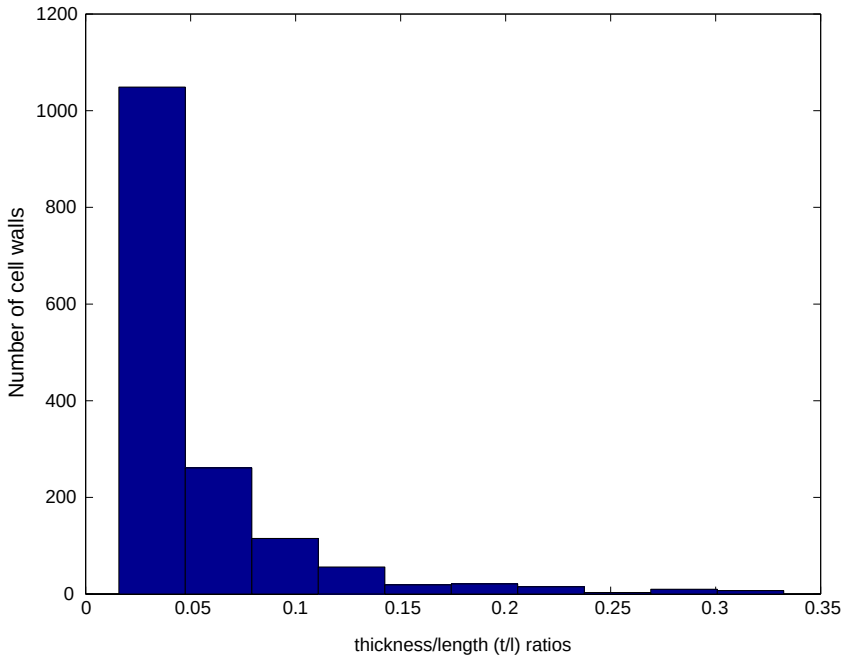

Fig. 2. Histogram of thickness/length (t/l) ratio for the cell walls for the structure shown in Fig. 1. The distribution indicates that only 10.09% elements have t/l ratio greater than 1/10 with 2.5% elements have t/l ratio greater than 1/5. Therefore, most of the cell walls (about 90%) have t/l ratio less than 1/10.

Table 1
Geometric and material data for the beam shown in Fig. 1

Geometric data	
Length of the model L	600 mm
Overall depth in the transverse direction D	50 mm
Width perpendicular to the plane of paper	Unity
Length of the cell wall material $\sum_i l_i$	7575.4 mm
Thickness of the cell walls t	0.175 mm
Number of nodes	1148
Number of elements	1556
Total degrees-of-freedom	3444
Material data	
Modulus of elasticity of the cell wall material (aluminium) E_s	70 GPa
Density of the cell wall material (aluminium) ρ_s	2700 kg/m^3

90%) have a t/l ratio of 1:10 or less. A histogram of the distribution of the thickness to length ratio is plotted in Fig. 2. Note the strong skewness towards the left end of the histogram that represents thin long beams.

The geometric and material data of the beam are presented in Table 1. We have taken the thickness as the same for all the cell walls. The external dimensions of the cellular beam are L and D in the axial and transverse directions giving an L/D ratio of 12 for the model. The beam has over 500 cells. The area fraction of the solid is calculated as

$$\frac{\rho^*}{\rho_s} = \frac{t \times \sum_i l_i}{L \times D}, \tag{30}$$

where ρ^* is the effective density of the overall structure. The relative density which is the same as the area fraction is about 0.044 for the example of Fig. 1.

To simulate the fixed end, all the degrees-of-freedom at the left end of the cellular beam are fixed after assembling the global stiffness and mass matrices. The continuum modes are obtained from the finite element analysis of a single fixed-free beam having the same macroscopic dimensions as the cellular beam. A small size finite element model having twelve elements with cubic interpolation is used to calculate the continuum modes. Mapping on the lines of Eq. (6) is achieved using Eqs. (4) and (5). The first ten continuum modes are chosen as the basis modes after pre-conditioning using Eq. (29). An in-house code was developed in MATLAB [24] for predicting the natural frequencies and the mode shapes using both the approximate method and the full-scale model.

Table 2 shows the first ten natural frequencies as calculated by solving the large eigenproblem (3) and by using the approximation of pre-conditioned continuum modes presented in this paper. The accuracy of the calculation is quite remarkable. The first nine modes show an error less than 1%.

Comparing mode shapes quantitatively is not as straightforward as comparing natural frequencies because of non-uniqueness of eigenmodes up to an arbitrary scaling. MAC (Modal Assurance Criterion) is frequently used to correlate the experimental mode shapes with those obtained by the finite element method [25]. In this paper, we use this established method to

Table 2
Comparison between the natural frequencies as calculated from the full model (Eq. (3)) and the approximation based on pre-conditioned continuum modes for the cellular beam in Fig. 1

Mode no.	Natural frequency (Hz)	Approximate frequency (Hz)	Relative error (%)
1	4.79	4.79	-4.89×10^{-7}
2	29.40	29.40	-5.51×10^{-6}
3	80.50	80.50	-4.21×10^{-4}
4	102.51	102.51	-4.78×10^{-4}
5	143.82	143.83	-3.96×10^{-3}
6	213.35	213.41	-2.69×10^{-2}
7	317.00	317.68	-2.14×10^{-1}
8	324.64	324.82	-5.77×10^{-2}
9	393.06	394.01	-2.41×10^{-1}
10	493.45	526.98	-6.80

correlate the mode shapes obtained from the proposed approximation with finite element simulated modes.

The MAC matrix **C** has the entries given by [25]

$$C_{ij} = \frac{(|\mathbf{u}_i^{\mathrm{T}}\mathbf{q}_j|)^2}{(\|\mathbf{u}_i\|)^2(\|\mathbf{q}_j\|)^2}. \tag{31}$$

The diagonal terms of the matrix represent the correlation between two eigenvectors associated with the same mode, whereas the off-diagonal terms reflect the correlation between the cross-eigenvectors. For best correlation, the value of C_{ij} will be 1, whereas the value of C_{ij} will be zero for poorest or no correlation. A grey scale with black colour for $C_{ij} = 1$ and white colour for $C_{ij} = 0$ is used. The intermediate shades indicate the correlation proportionately.

The relative magnitudes of the quantity C_{ij} in Fig. 3 reflect the correlation between the *original* assumed continuum modes without pre-conditioning with the finite element modes. Similarly, Fig. 4 is plotted with C_{ij}s calculated on the basis of the proposed reduced order model after pre-conditioning and the finite element modes. Note the improvement in the correlation due to the pre-conditioning and the application of Rayleigh's variational principle.

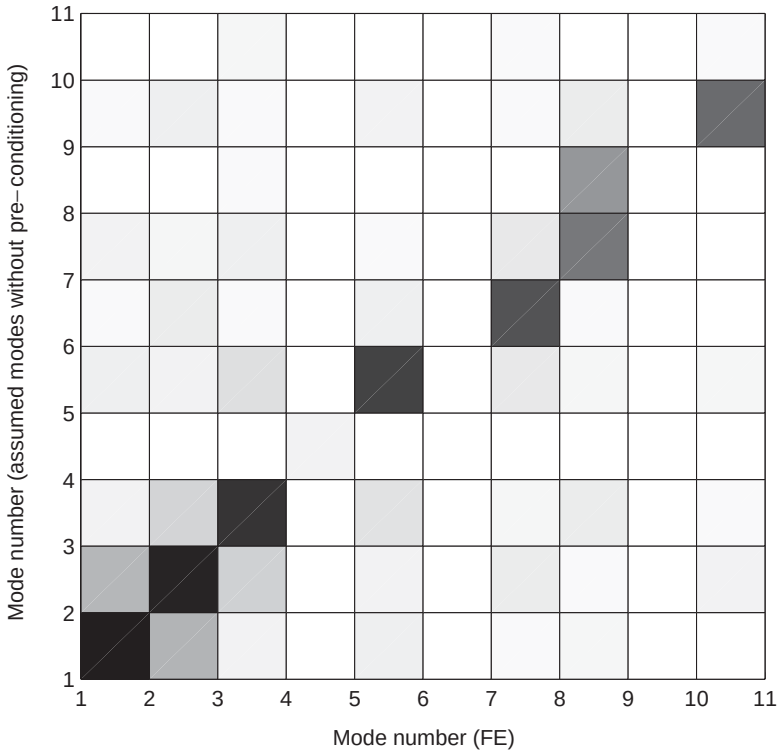

Fig. 3. MAC plot correlating the continuum assumed modes and the finite element modes. The dark blocks on the diagonal indicate good correlation for the first few modes; yet the predicted frequencies based on these assumed modes are very inaccurate.

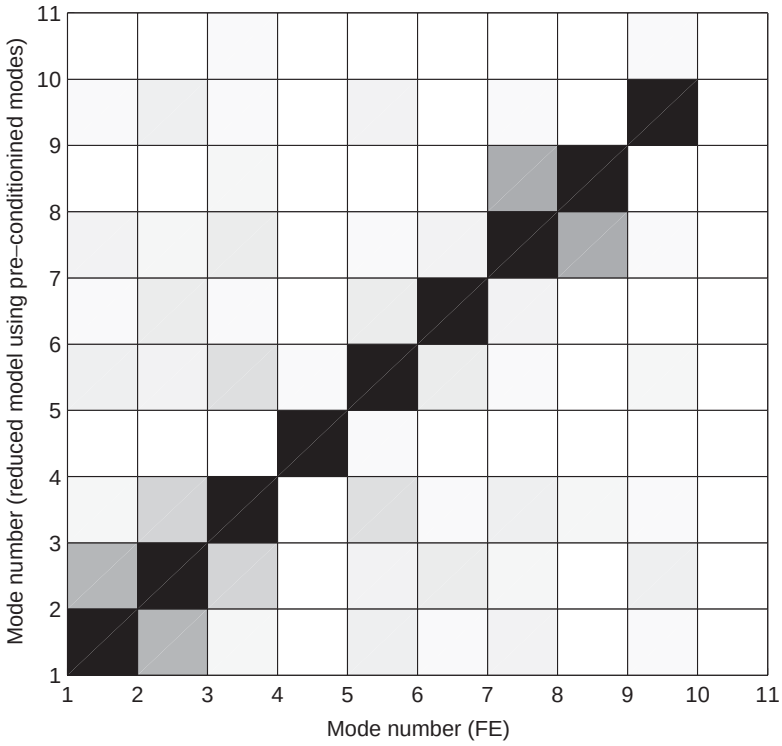

Fig. 4. MAC plot representing correlation between the two sets of eigenvectors as calculated by the finite element and the reduced order model. The dark blocks on the diagonal show excellent correlation up to the eighth mode. Correlation for the ninth mode is not so good, whereas the tenth mode shows poor correlation.

As a second method to compare the two eigenvectors [25], an eigenvector obtained from the reduced order model is plotted against the corresponding eigenvectors from the full-scale model in Fig. 5. If the points fall around the straight line passing through the origin at an orientation of 45°, a good correlation is indicated. The pair of two eigenvectors associated with the first, eighth, ninth and the tenth mode are plotted in Fig. 5.

The plot shows an excellent correlation for the first mode pair. The correlation up to the eighth mode is found to be very good. The ninth mode does not correlate so well. In the case of the tenth mode, the approximate mode is poorly correlated with the eigenvector of the full-scale model. The natural frequency predicted based on the approximate mode is about 7% higher than the corresponding finite element value. Considering that only ten modes are used in the calculation, and the correlation of the tenth assumed mode is poor with the corresponding actual mode, the accuracy is surprisingly good. More number of modes are to be included in the basis for improving the last mode.

The flop counts for the full-scale problem are compared with those of the reduced order problem in Table 3. The full-scale model is of size 3444×3444, whereas the continuum mode based reduced order model is of size 10×10. In view of this, only 10 modes were extracted while solving the full-scale problem (3) using a sparse solver in MATLAB.

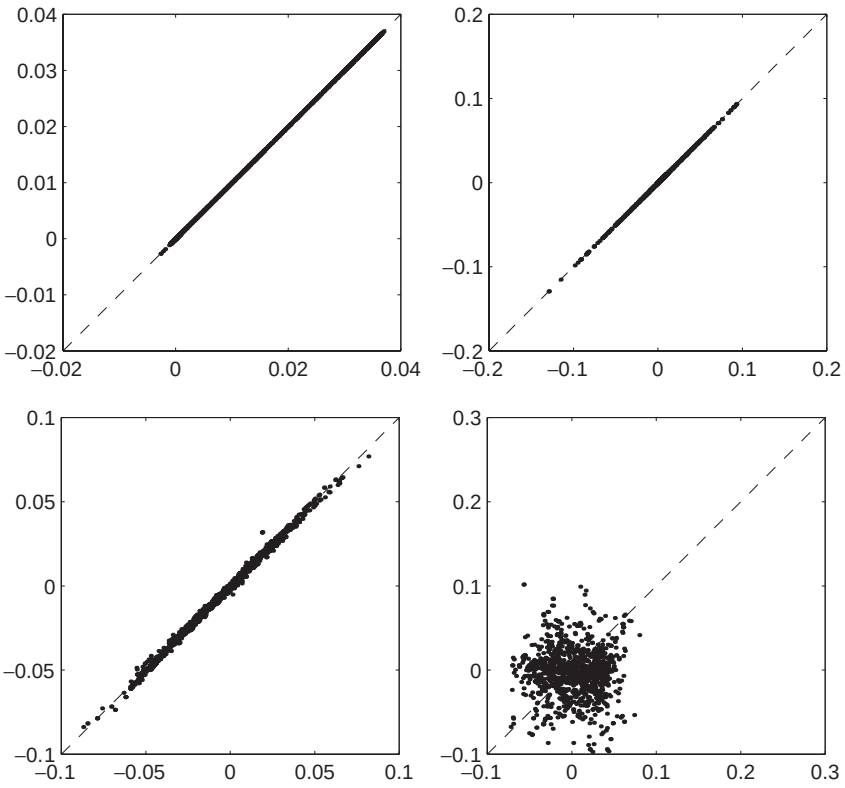

Fig. 5. The straight line correlation plot for the first (top left), eighth (top right), ninth (bottom left) and the tenth (bottom right) mode, respectively. Note the degradation in the correlation with the mode number.

Table 3
Comparison of the floating point operations for the full-scale problem (Eq. (3)) and the approximation using the pre-conditioned continuum modes for three cases. Note that calculations of eigenvalues and eigenvectors for the reduced model include all the stages starting from the generation of the pre-conditioned assumed modes up to the prediction of the approximate frequencies and modes

Degrees-of-Freedom		Floating point operations			% of full scale calculations
		Generation of of **K** & **M**	Calculations of frequencies and modes	Total calculations	
1431	Reduced model	1.20×10^5	6.74×10^6	6.86×10^6	11.39%
1431	Full model	1.20×10^5	6.01×10^7	6.03×10^7	100%
3444	Reduced model	3.14×10^5	2.08×10^7	2.11×10^7	9.58%
Example 1 (Section 4.1)					
3444	Full model	3.14×10^5	2.20×10^8	2.20×10^8	100%
4962	Reduced model	4.54×10^5	3.37×10^7	3.42×10^6	7.49%
4962	Full model	4.54×10^5	4.56×10^8	4.57×10^8	100%

Two other models were generated by replacing the microstructure of the present example by different cellular topologies. The degrees-of-freedom of the models were 1431 and 4962, respectively. The basis continuum modes used in Example 1 were used for these models as the external dimensions of the beam were the same. Therefore, the continuum modes need to be generated only once for structures with the same overall dimensions but filled with various cellular topologies. This is another advantage of the method leading to further computational savings in such cases. However, flops required for the generation of the continuum modes were included in the comparison for all the reduced order models.

Table 3 shows that the total flops required for the approximate method in the case of Example 1 is only 9.58% of that for the whole model. Break-up of flops indicates that the generation of full **K** and **M** is much cheaper, it requires flops less than 1% when compared to the full model calculations. Table 3 also indicates that the savings will be a lot more for structures with higher degrees-of-freedom. Sometimes, a single mode calculation is very economical when we use the assumed mode directly into Rayleigh's quotient. We implemented this for the first mode and the approximation matched the value obtained from the full-scale calculation within 0.000001%.

The first five modes of vibration of the structure shown in Fig. 1 are presented in Fig. 6. The first three modes resemble those of a solid fixed-free beam. These three modes are primarily bending modes. The fourth mode resembles the first axial mode in tension–compression for a fixed-free elastic rod with axial degrees-of-freedom. The fifth mode is the fourth mode in the bending series. The approximate method has predicted both the bending and the axial modes accurately. The figures broadly justify the idea of using the continuum modes as the assumed modes for cellular structures.

4.2. Example 2: L-beam

The second example of an L-beam is shown in Fig. 7. To generate the structure of this shape filled with cellular material, we first created a large block of Voronoi cells. Then a structure of the required L-shape was cut out of this rectangular block. Cell walls having very small length were created during the model generation process. They were eliminated in a similar way as was done for the cantilever beam. About 3% of the cell walls needed deleting from the mesh. The thickness of the cell walls was chosen such that the minimum t/l ratio is $1/3$. The distribution of length thus generated indicates that only 7.4% elements have t/l ratios greater than $1/10$ with 2.3% elements have t/l ratio greater than $1/5$. Therefore, about 92.6% of the cell walls have a t/l ratio less than $1/10$. Hence, the shear effect can be neglected for most cell walls.

The beam is composed of approximately 600 cells. The geometric data for the L-beam are presented in Table 4. The material properties are the same as those used for the cantilever beam. The two arms of this L-beam have a L/D ratio about 8.5. The area fraction of the cellular solid calculated from Eq. (30) is about 0.025. The continuum modes were calculated from a finite element analysis of the L-shaped skeleton.

Table 5 shows a comparison of the natural frequencies as calculated from Eq. (3) with those calculated on the basis of the pre-conditioned continuum modes. The agreement is excellent again, with frequencies well within 1% up to the eighth mode. To assess the accuracy of the modes obtained via the reduced order model, MAC matrix **C** is calculated to correlate the reduced order modes and the finite element modes. The MAC plot for the L-beam is shown in Fig. 8. The figure

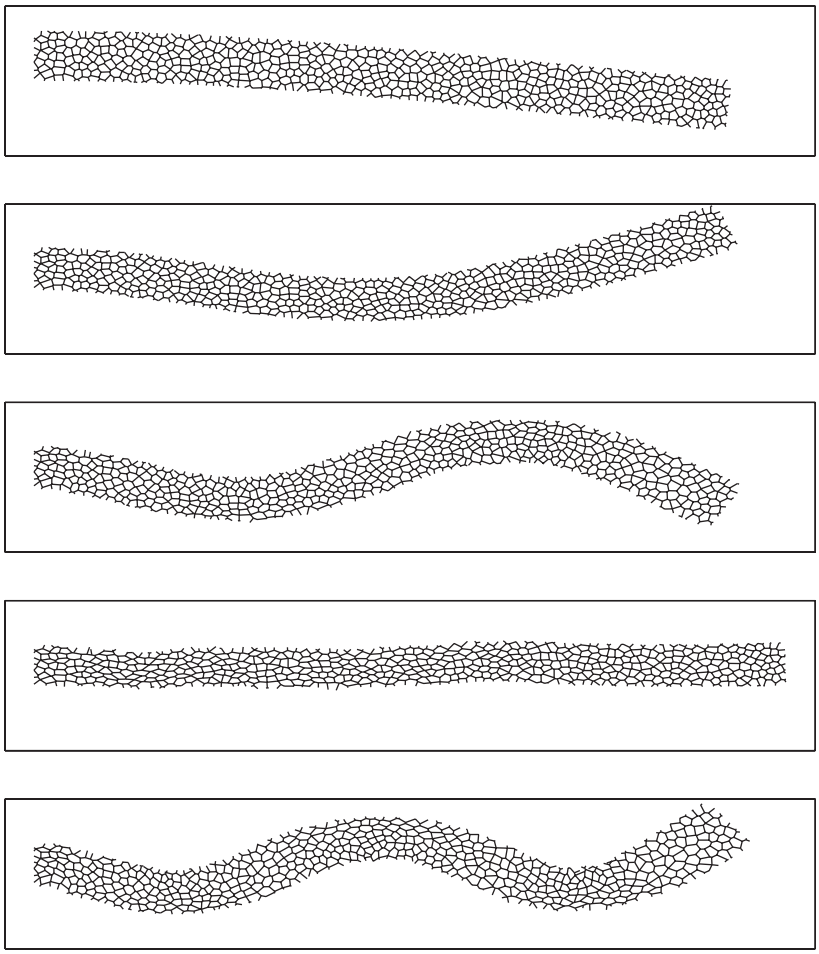

Fig. 6. This figure shows the first five mode shapes of the cantilever beam shown in Fig. 1. The modes are plotted on the basis of the finite element eigenvectors. The deflected shape of the first mode resembles the first flexural mode of a solid fixed-free beam. The second, third and the fifth mode resemble the second, third and the fourth flexural mode of a cantilever respectively. In contrast to the previous bending modes, the fourth mode is primarily an axial mode. This mode resembles the first normal mode of a rod in axial vibration.

indicates excellent correlation up to the eighth mode. The ninth and the tenth mode show poor correlation as expected.

The size of the eigenvalue problem is reduced to 10×10 from 3837×3837 for this example. The total floating point operations involved in the approximate method (3.74×10^7) is less than 10% of the operations required for the full model (3.93×10^8). Therefore, substantial computational saving is achieved for such a complex structure. Similar to the previous example, only ten modes of the full model were obtained using a sparse solver.

The L-beam with identical arms will have degenerate modes of multiplicity two if the beams have only bending degrees-of-freedom. This is because the corner will act as a pin joint with only

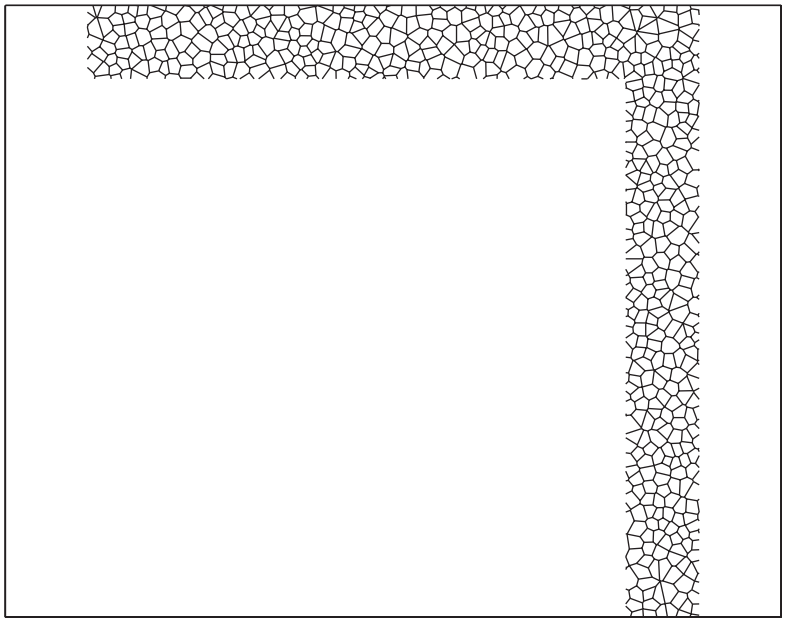

Fig. 7. An L-beam composed of irregular cells. Note that the left-most and the bottom-most boundary are fixed such that the displacements and rotations of all the nodes on these two boundaries are zero.

Table 4
Geometric data for the L-beam shown in Fig. 7

External length of each arm of the model	1250 mm
Internal length of each arm of the model	1100 mm
Overall depth perpendicular to the length direction D	150 mm
Width perpendicular to the plane of paper	Unity
Length of the cell wall material $\sum_i l_i$	27171.2 mm
Thickness of the cell walls t	0.33 mm
Number of nodes	1279
Number of elements	1696
Total degrees-of-freedom	3837

rotations allowed and the system will have two coincident natural frequencies. Each of these corresponds to a beam fixed at one end and pinned at the other. When axial degrees-of-freedom are allowed and when two arms are not identical (as in case of cellular arms) the degeneracy is broken and we expect to obtain frequencies in doublets. Each pair originates from one set of degenerate modes.

When we look at the frequencies of the cellular L-beam (see Table 5), we find a similar pattern but the frequencies are not that close. For example, the ratio of the first and the second frequencies is 1.54. The third and the fourth are the closest having a ratio equal to 1.08, whereas the fifth and the sixth possess a ratio of 1.24. The originally degenerate modes have split quite far

Table 5
Comparison of the natural frequencies as calculated from the full model (Eq. (3)) and the approximation using the pre-conditioned continuum modes for the L-beam shown in Fig. 7

Mode no.	Natural frequency (Hz)	Approximate frequency (Hz)	Relative error (%)
1	4.25	4.25	-1.86×10^{-4}
2	6.54	6.54	-9.26×10^{-4}
3	11.87	11.88	-1.01×10^{-2}
4	12.85	12.85	-8.54×10^{-3}
5	14.75	14.76	-8.52×10^{-3}
6	18.24	18.25	-2.84×10^{-2}
7	25.41	25.44	-1.27×10^{-1}
8	30.14	30.22	-2.51×10^{-1}
9	39.55	41.18	−4.13
10	39.96	42.22	−5.66

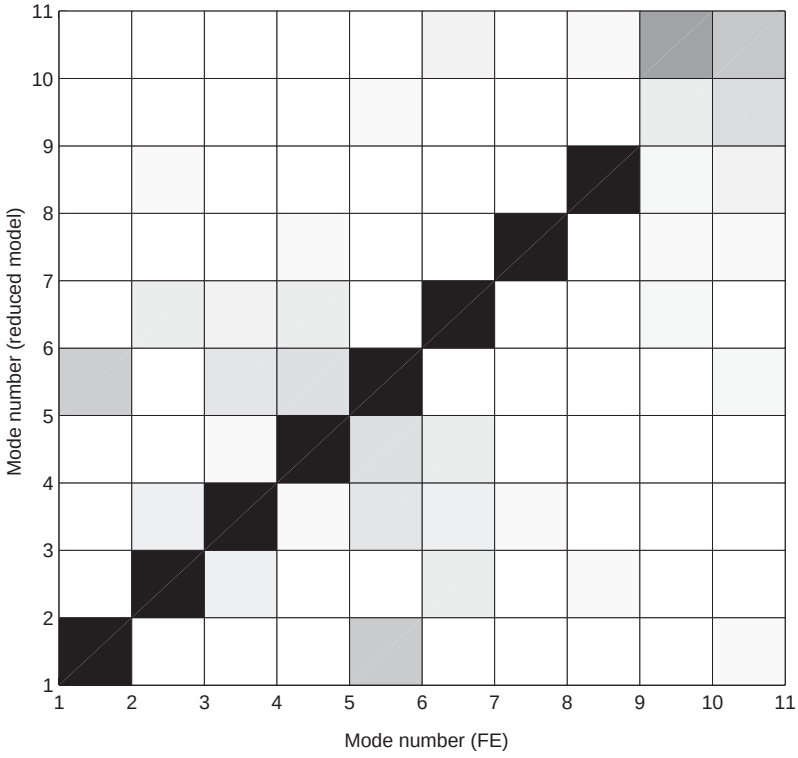

Fig. 8. MAC plot representing correlation between the modes calculated by the finite element and the approximate method of the L-beam structure. The dark blocks on the diagonal show excellent correlation up to the eighth mode. The ninth and the tenth modes show poor correlations.

because the two arms of the L-beam possess different microstructure. As a result, their individual natural frequencies are not the same.

Figs. 9–13 show the first five natural modes of the L-beam. The mode shapes as obtained from the full-scale finite element analysis using Eq. (3) and those obtained from the reduced order model almost coincide. Therefore, the mode shapes are displayed based on the eigenvectors calculated for the full model. The overall mode shapes of the cellular L-beam are similar to the corresponding modes of a solid L-beam.

The first two modes are overall bending modes (see Figs. 9 and 10). The third and the fourth mode resemble each other (see Figs. 11 and 12). The horizontal arm is in the stretching–compression mode of vibration and the vertical arm is in flexural vibration in the case of the third mode. The opposite happens for the fourth mode where the stretching–compression mode of vibration is observed in the vertical arm and the flexural mode in the other. The fifth mode (see Fig. 13) is primarily a bending mode with each arm corresponding to the second mode of vibration for a fixed-pinned beam.

Cellular metals are often used as the core for sandwich constructions. To model such composites, one could take two alternative routes. While the core can be modelled in a manner similar to that used for illustrations in this paper, the external plates could be modelled using additional elements (beams for planar models of foams; plates for three dimensional geometry). If the external plates are not isotropic (as often is the case), the relevant anisotropy (usually orthotropy) can be accounted for by appropriately choosing the elements that represent the face-plates. An alternative to this approach could be to use analytical models that combine the face-plate geometry and properties with those of the core—the core being represented by an effective

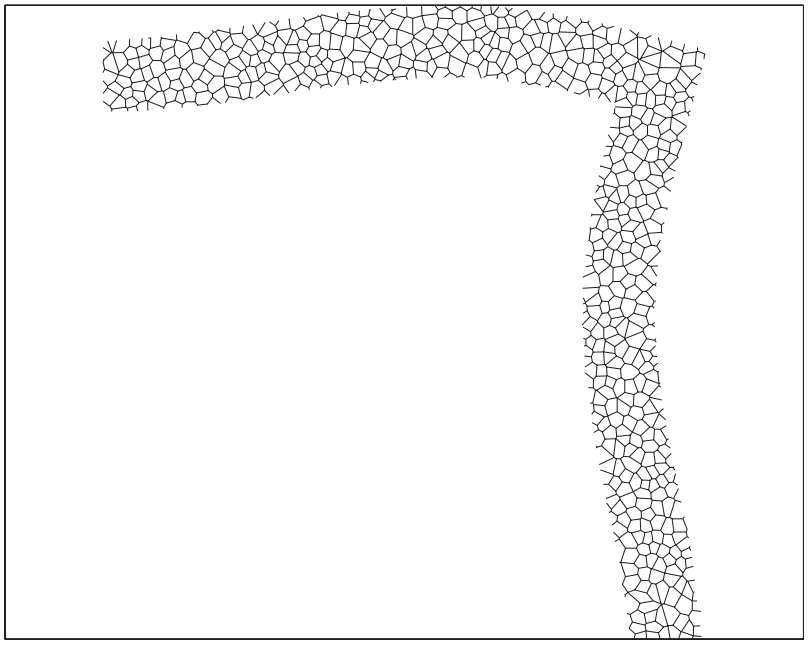

Fig. 9. The first mode of free vibration of the L-beam. All the displacements are plotted in exaggerated scale.

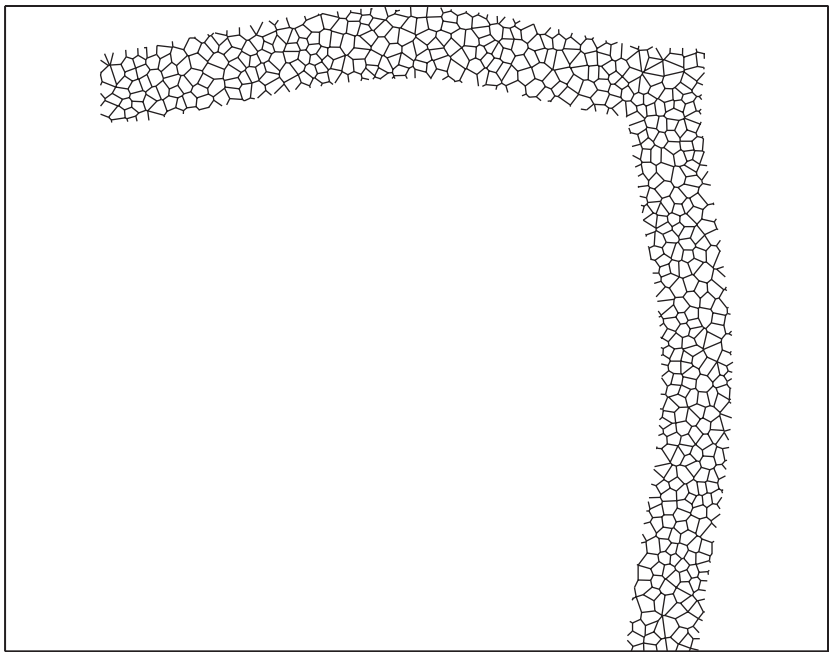

Fig. 10. The second mode of vibration. This mode is also a flexural mode, similar to the first mode, but the phase of vibration in the two limbs of the structure is opposite of the mode presented in Fig. 9.

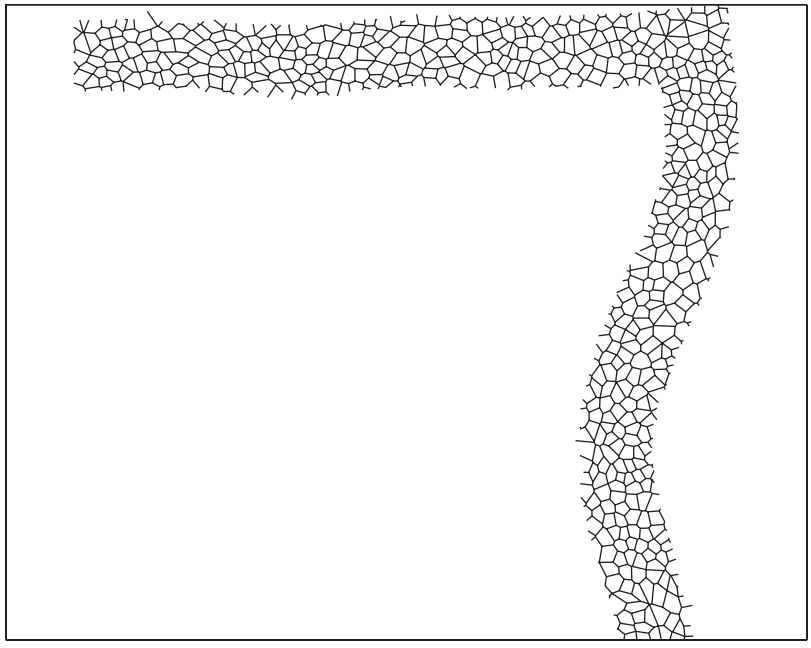

Fig. 11. The third mode of vibration. The horizontal arm is in stretching-compression mode of vibration whereas the vertical arm is in flexural vibration.

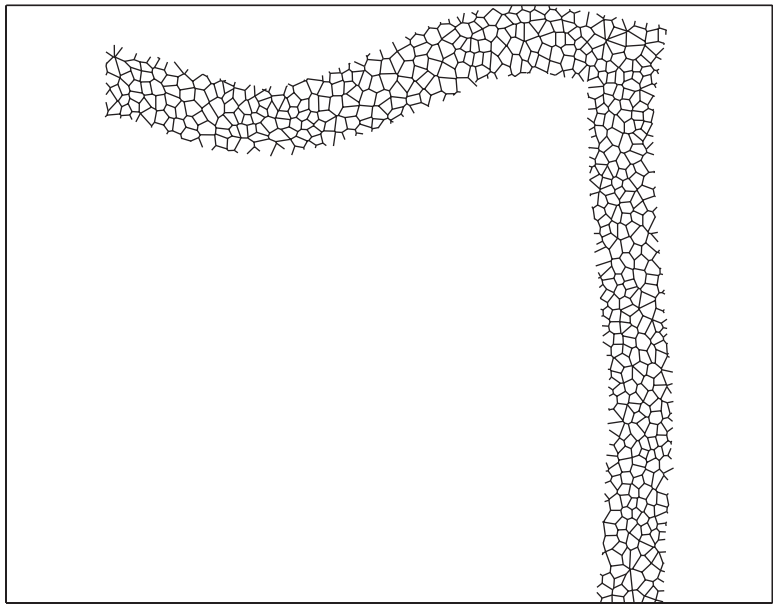

Fig. 12. The fourth mode of vibration. This mode is similar to the third mode, the difference being that the vertical arm is in stretching–compression mode of vibration in this mode. The horizontal arm is in flexural mode of vibration.

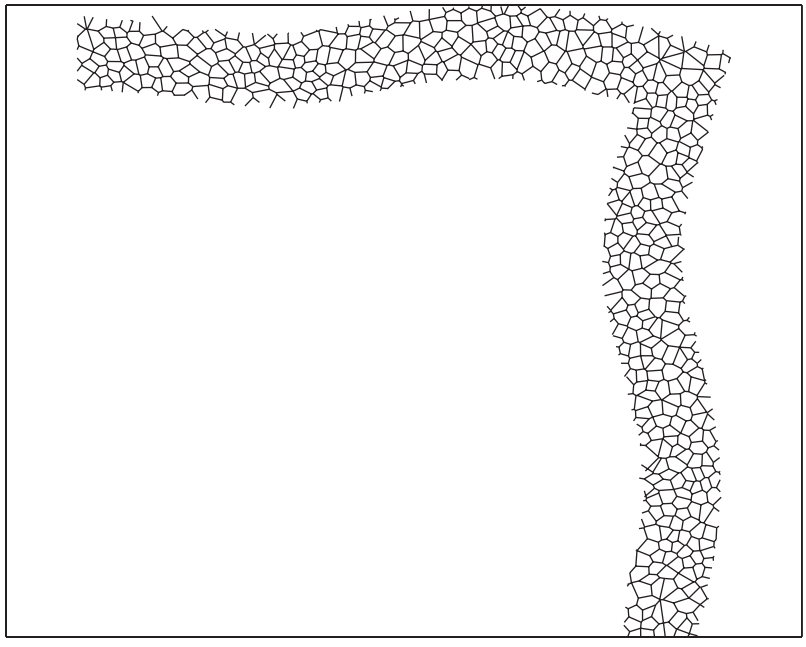

Fig. 13. The fifth mode of vibration. It is primarily a bending mode with each arm corresponding to the second mode of vibration for a fixed-pinned beam.

medium. In this case, the shear modulus of the core will be of great importance. We have not undertaken the task of modelling such composites since the main objective of this paper is to present an approximation method and not to model cellular composites.

5. Conclusions

A realistic representation of cellular structures requires modelling structures with a number of cells. As a result, the eigenvalue problem associated with the free vibration is large, and hence, computationally demanding. An approximate method was presented in this paper to overcome this difficulty. The proposed method can be used for approximately calculating the first few natural frequencies and the associated modes for the cellular structures with substantial computational saving. The method is based on the assumption that macroscopically cellular structures behave as a homogeneous continuum for low frequency dynamics. Assumed modes based on the continuum modes were used as the basis in this method. The frequencies and the mode shapes were predicted accurately using Rayleigh's variational principle.

A direct use of the assumed modes for the approximation leads to large errors. It was shown to be due to the presence of small high-frequency mode components in the assumed modes. A method based on inverse power iterations was used to pre-condition the assumed modes successfully. Further, a sensitivity analysis was performed to study the effect of an arbitrarily chosen vector on Rayleigh's approximation. We found that even small errors in the trial vector can ruin the predictions unless care is taken in pre-conditioning the assumed continuum modes.

Two examples were given for planar structures to demonstrate the working of the method. Structures made of irregular cells were analysed. A significant model-order reduction was achieved by the proposed method without compromising the accuracy. The method may be applicable for more complex structures.

Acknowledgements

This work was supported by the EPSRC Grant no GR/R45895/01.

References

[1] L.J. Gibson, M.F. Ashby, G.S. Schajer, C.I. Robertson, The mechanics of two-dimensional cellular materials, *Proceedings of the Royal Society of London A* 382 (1982) 25–42.

[2] W.E. Warren, A.M. Kraynik, Foam mechanics: the linear elastic response of two-dimensional spatially periodic materials, *Mechanics of Materials* 6 (1987) 27–37.

[3] S.T. Gulati, Effects of cell geometry on thermal shock resistance of catalytic monoliths, *Automotive Engineering Congress and Exhibition Society of Automotive Engineers*, Detroit, Michigan, 1975, paper 750171, pp. 1–9.

[4] F. Scarpa, P. Panayiotou, G. Tomlinson, Numerical and experimental uni-axial loading on in-plane auxetic honeycombs, *Journal of Strain Analysis for Engineering Design* 35 (5) (2000) 383–388.

[5] G. Menges, F. Knipschild, Estimation of mechanical properties for rigid polyurethane foam, *Polymer Engineering Science* 15 (1975) 623–627.

[6] W.L. Ko, Deformation of foamed elastomers, *Journal of Cellular Plastics* 1 (1965) 45–50.
[7] L.J. Gibson, M.F. Ashby, *Cellular Solids: Structure and Properties*, second ed., Cambridge University Press, Cambridge, 1997.
[8] L.J. Gibson, Mechanical behaviour of metallic foams, *Annual Review of Material Science* 30 (2000) 191–227.
[9] R.M. Christensen, Mechanics of cellular and other low-density materials, *International Journal of Solids and Structures* 37 (2000) 93–104.
[10] J.L. Grenestedt, Effective elastic behaviour of some models for 'perfect' cellular solids, *International Journal of Solids and Structures* 36 (10) (1999) 1471–1501.
[11] M.J. Silva, W.C. Hayes, L.J. Gibson, The effect of the non-periodic microstructure on the elastic properties of two-dimensional cellular solids, *International Journal of Mechanical Sciences* 37 (1995) 1161–1177.
[12] H.X. Zhu, J.R. Hobdell, A.H. Windle, Effects of cell irregularity on the elastic properties of 2D Voronoi honeycombs, *Journal of The Mechanics and Physics of Solids* 49 (2001) 857–870.
[13] M.J. Silva, W.C. Hayes, L.J. Gibson, The effects of non-periodic microstructure and defects on the compressive strength of two-dimensional cellular solids, *International Journal of Mechanical Sciences* 39 (1997) 549–563.
[14] A.E. Simone, L.J. Gibson, Effects of solid distribution on the stiffness and strength of metallic foams, *Acta Materialia* 46 (1998) 2139–2150.
[15] J.L. Grenestedt, Influence of wavy perfections in cell walls on elastic stiffness of cellular solids, *Journal of The Mechanics and Physics of Solids* 46 (1998) 29–50.
[16] C. Chen, T.J. Lu, N.A. Fleck, Effect of imperfections on the yielding of two-dimensional foams, *Journal of The Mechanics and Physics of Solids* 47 (1999) 2235–2272.
[17] S.J. Hollister, N. Kikuchi, Homogenisation theory and digital imaging: a basis for studying the mechanics and design principles of bone tissue, *Biotechnology and Bioengineering* 43 (1994) 586–596.
[18] E.J. Garboczi, A.R. Day, An algorithm for computing the effective linear elastic properties of heterogeneous materials: 3-D results for composites with equal phase Poisson ratios, *Journal of the Mechanics and Physics of Solids* 43 (1995) 1349–1362.
[19] S. Torquato, L.V. Gibiansky, M.J. Silva, L.J. Gibson, Effective mechanical and transport properties of cellular solids, *International Journal of Mechanical Sciences* 40 (1998) 71–82.
[20] X.L. Wang, W.J. Stronge, Micropolar theory for a periodic force on the edge of elastic honeycomb, *International Journal of Engineering Sciences* 39 (2001) 821–850.
[21] W.E. Baker, T.C. Togami, J.C. Weydert, Static and dynamic properties of high-density metal honeycombs, *International Journal of Impact Engineering* 21 (1998) 149–163.
[22] L. Meirovitch, *Elements of Vibration Analysis*, first ed., McGraw-Hill Book Company, New York, 1975.
[23] R.L. Fox, M.P. Kapoor, Rate of change of eigenvalues and eigenvectors, *AIAA Journal* 6 (1968) 2426–2429.
[24] MATLAB 5.3, *User's Guide*, The Mathworks, Inc., Natick, MA, 1995.
[25] D.J. Ewins, *Modal Testing, Theory, Practice and Applications*, second ed., Research Studies Press, Baldock Herts, 2000.